Excerpt from the Proceedings of the 2011 COMSOL Conference in Tokyo

Tertiary Current Distributions on Rotating Electrodes

Lizhu Tong[1]
[1]Kesoku Engineering System Co., Ltd.
1-9-5 Uchikanda, Chiyoda-ku, Tokyo 101-0047, Japan, tong@kesco.co.jp

Abstract: The tertiary current distributions on rotating electrodes are studied in this work. An acid copper sulfate electrolyte is used within an electrochemical cell of practical dimensions. The distributions of ion concentrations are obtained by the two-dimensional fluid flow simulation and the solution of mass-transport equations based on axial symmetry. The calculated concentration boundary layer thicknesses agree well with those from Levich equation. It is found that the tertiary current distribution on working electrode is affected by the rotating velocity of electrode and the effect disappears with the increase of rotating velocity up to 1000 rpm in comparison with the secondary current distribution. The tertiary current distributions for three types of working electrode are calculated and an improved shape of working electrode is proposed.

Keywords: Rotating electrode, Tertiary current distribution, Concentration boundary layer, Shape of working electrode.

1. Introduction

Rotating electrodes are primarily employed to impose forced convection on an electrode reaction, to negate vagaries of free convection that can arise as a result of thermal and density changes in the vicinity of the electrode/ electrolyte interface [1].

Hydrohynamic electrochemical processes with the rotating electrode have been described for mass-transport studies [2,3]. Dong and co-workers [2] solved the velocity and pressure profiles in the electrolyte due to a rotating electrode, in which the hydrodynamic models were coupled with a mass-transport model for oxygen reduction reaction at the surface of the rotating electrode. Barcia and co-workers [3] studied the frequency response of the limiting current to a sinusoidal speed modulation at a rotating hemispherical electrode (RHSE). The unsteady hydrodynamic problem and the unsteady mass transport problem were solved, in which the theoretical expression of the electrohydro-dynamic impedance (EHD) was presented.

It is known that at currents much below the limiting current, the solution of the current density can be regarded as the potential theory problem [4], *i.e.*, the current distribution is determined by the ohmic potential drop in the solution and the electrode overvoltage, termed as secondary current distribution, in which the current distribution determined only by the ohmic potential drop in the solution is termed as primary current distribution. However, in the cases close to the limiting current, diffusion and convective transport become essential [5], which was termed as the tertiary current problem by Averill and Mahmood [6]. Low and co-workers [7] performed the simulations of the non-uniform current, potential and concentration distributions along the cathode of a rotating cylinder Hull (RCH) cell. They examined the primary, secondary, and tertiary current distributions. In their research, the concentration distribution was solved only within the boundary layer using a Laplace equation $\nabla^2 c = 0$, where c is the concentration. Outside the boundary layer the concentration was assumed to be constant, *i.e.*, the bulk concentration. The thickness of the boundary layer was determined by the Eisenberg's empiric correlation. Unfortunately, the thickness of concentration boundary layer is usually unknown, which depends on fluid dynamics around working electrode.

In this work, we coupled the calculations of fluid flows and current distributions. The effect of fluid flows on the current distributions on electrode surface was presented. The tertiary current distributions were compared with the secondary current distributions and the different shapes of working electrodes were analyzed and discussed.

2. Numerical Model

The model geometry used in this work is shown in Fig. 1. The dimensions of the electro-chemical cell are determined by practical measurement using glass beaker [8]. It is well

known that the Reynolds number can be calculated by [9]

$$R_e = \rho\omega {r_d}^2/\mu. \quad (1)$$

The critical Reynolds number for the transition from laminar to turbulent regimes is 10^5 for rotating disk electrodes (RDE), 2×10^4 for rotating hemispheral electrodes (RHSE), 6×10^4 for rotating cone electrodes (RConE) [1]. Since the rotating disk considered $r_d = 3\times10^{-3}\mathrm{m}$, the Reynolds number *Re* = 1881 for rotating velocities ω = 2000 rpm (*i.e.*, 209 rad/s) and kinematic viscosity $\nu(=\mu/\rho) = 1\times10^{-6}\mathrm{m}^2/\mathrm{s}$, so that in this work the laminar flows are taken into account by [10]

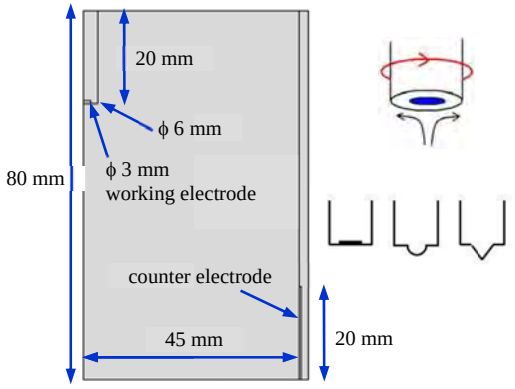

Figure 1. Schematic of the rotating electrodes used in this work.

Continuity equation

$$\frac{\partial\rho}{\partial t} + \nabla\cdot(\rho\mathbf{u}) = 0, \quad (2)$$

Momentum equation

$$\rho\frac{\partial\mathbf{u}}{\partial t} + \rho\mathbf{u}\cdot\nabla\mathbf{u} = -\nabla p + \nabla\cdot\Big(\mu(\nabla\mathbf{u} + (\nabla\mathbf{u})^T) - \frac{2}{3}\mu(\nabla\cdot\mathbf{u})\mathbf{I}\Big) + \mathbf{F}, \quad (3)$$

where ρ is the density, **u** is the velocity vector, p is the pressure, **F** is the volume force vector, **I** is the identity matrix.

The material balance equation for the species *i* in the electrolyte is calculated [5,10,11]

$$\frac{\partial c_i}{\partial t} + \nabla\cdot\left(-D_i\nabla c_i - z_i u_{m,i} F c_i \nabla\phi_l + c_i\boldsymbol{u}\right) = R_{i,tot}, \quad (4)$$

where c_i is the concentration of species *i*, D_i is the diffusion coefficient of species *i*, z_i is the charge number of species *i*, $u_{m,i}$ is the mobility of species *i*, *F* is Faraday's constant, and ϕ_l is the electrical potential. The current density $\mathbf{i}_l$ in the electrolyte is

$$\mathbf{i}_l = F\sum_{i=1}^{n} z_i\left(-D_i\nabla c_i - z_i u_{m,i} F c_i\nabla\phi_l\right), \quad (5)$$

and then the charge balance in the electrolyte becomes

$$\nabla\cdot\mathbf{i}_l = Q_l, \quad (6)$$

where, Q_l can here be any source or sink. Also, the equation for the electroneutrality condition is considered by

$$\sum z_i c_i = 0. \quad (7)$$

It is known that the local current density on the electrode is related to the local overvoltage, η on the electrode, which is the potential difference between the electrode, *V*, and the solution adjacent to the electrode, ϕ_0, *i.e.*, $\eta = V - \phi_0$. The overvoltage can be adequately related to the magnitude of the local current density through the Tafel approximation in case that the concentration gradient is negligible [7]

$$i = -i_0\exp(-\eta/b_c), \quad (8)$$

where b_c is the Tafel slope, and i_0 is the exchange current density. By eq. (8), the secondary current distribution involving charge transfer effects is calculated.

In this work the tertiary current distribution involving the effects of concentration gradient is solved by the modified Tafel approximation [7]

$$i = -i_0\exp(-\eta/b_c)c_w/c_b, \quad (9)$$

where c_w is the surface concentration on electrode and c_b is the bulk concentration.

Eqs. (2)-(7) are solved using the finite element simulation software COMSOL Multiphysics 4.2. The calculation of fluid flows is coupled into the Electrodeposition module [10]. Eqs. (8) and (9) are used for the calculations of the secondary and tertiary current distributions, respectively. An acid copper sulfate electrolyte composed of $CuSO_4{\cdot}5H_2O$ of 75 g and H_2SO_4 of 190 g is taken into account in this work. The parameters considered are given in Table 1, which are

Table 1: Parameters used in the present research.

Rotating electrode
Diameter of disk: 6 mm
Diameter of working electrode: 3 mm
Rotating velocity: 20 rpm - 1300 rpm
Electrolyte properties
Kinematic viscosity: 9.76×10^{-7} m^2/s
Bulk concentration of cupric ions: 300 mol/m^3
Diffusion coefficient of cupric ions: 7.12×10^{-10} m^2/s
Electrolytic conductivity: 42.7 S/m
Electrode characteristics
Tafel slope: 0.0658 V
Exchange current density: 7.676 A/m^2

obtained from the previous experimental measurements [8].

3. Results

3.1 Simulation of fluid flows and concentration distributions

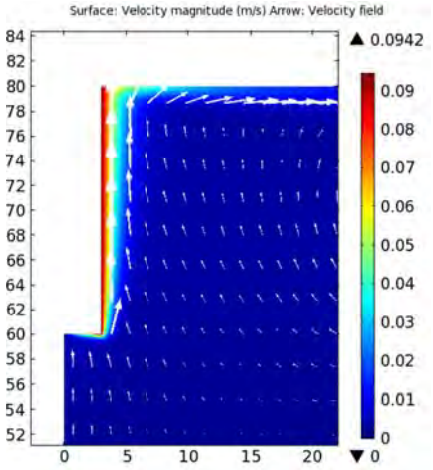

Figure 2. Velocity distribution around the rotating electrode at ω = 300 rpm.

The computations are performed for the distributions of fluid flows and concentrations around a rotating electrode at a rotating velocity from 20 rpm to 1000 rpm. The solved domain is limited up to the interface between air and solution. The boundary for the interface is regarded as free-slip wall and the bottom and side boundaries are stationary no-slip walls. The

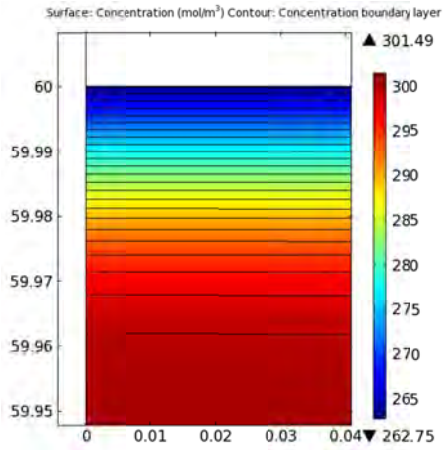

Figure 3. Concentration distribution around the working electrode at ω = 300 rpm.

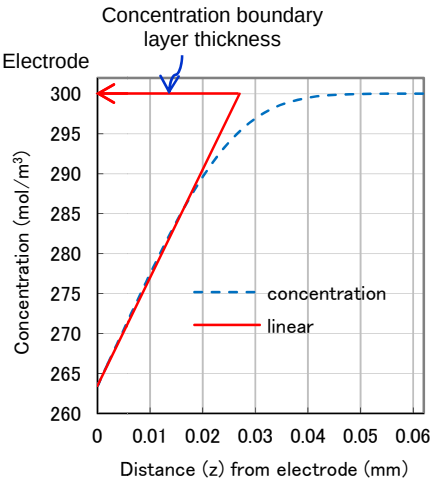

Figure 4. Concentration boundary layer thickness at the working electrode at ω = 300 rpm.

boundaries for electrode walls are defined as rotating no-slip walls with rotating velocity. Figure 2 shows the velocity distribution around the rotating electrode at ω = 300 rpm. The corresponding concentration distribution around the working electrode is shown in Fig. 3. In computations, the size of the first layer of mesh at the working electrode is set 1 μm so as to allow us to estimate the concentration boundary layer thickness from several to tens of microns. The concentration boundary layer thickness [11] is defined in Fig. 4 and the concentration distributions close to the surface of working electrode for different rotating velocities are

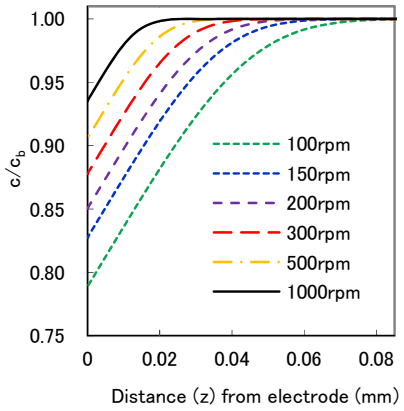

Figure 5. Concentration distributions at the working electrode for different rotating velocities.

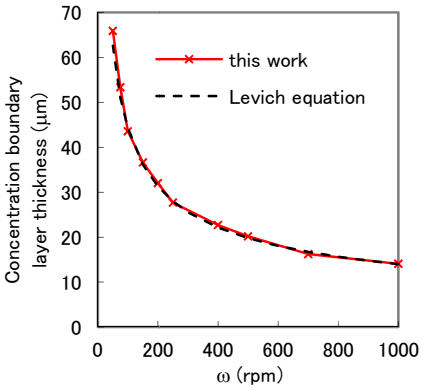

Figure 6. Concentration boundary layer thicknesses at a rotating velocity of 20-1000 rpm in comparison with those from Levich equation.

shown in Fig. 5. The thickness of the concentration boundary layer varies with the rotating velocity. The Levich equation is an empiric correlation for estimating the thickness for rotating electrodes [11]

$$\delta_N = 1.61\left(\frac{D}{\nu}\right)\left(\frac{\nu}{\omega}\right) \qquad (10)$$

The agreement between the present simulation and Levich equation is very good, as shown in Fig. 6.

3.2 Tertiary current distribution at the working electrode and its comparison with secondary current distribution

The tertiary current distribution around the

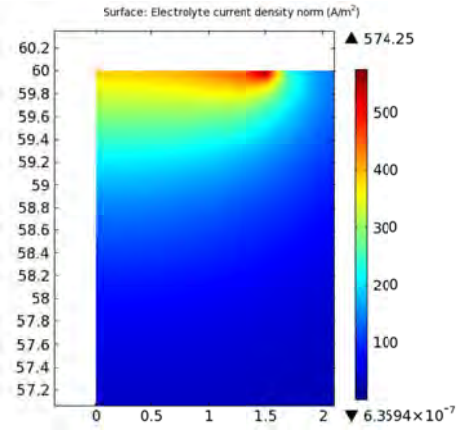

Figure 7. Tertiary current distribution around the working electrode at ω = 300 rpm.

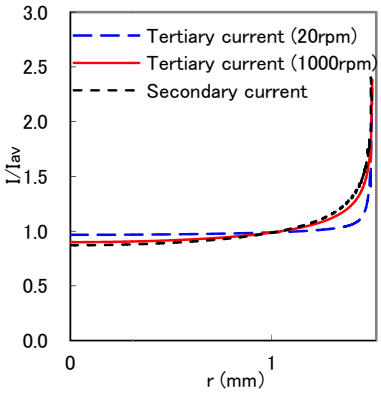

Figure 8. Tertiary current distribution at the working electrode in comparison with secondary current distribution. I_{av} is the average current density over the working electrode.

working electrode at ω = 300 rpm is shown in Fig. 7. The maximum current density is found to be located at the corner of working electrode. The comparison of tertiary current distributions and secondary current distribution at the working electrode is shown in Fig. 8. The effect of the rotating velocity of electrode to current distribution is large at the lower rotating velocity and the effect disappears when the rotating velocity is increased up to 1000 rpm in comparison with the secondary current distribution. It could be concluded that that rotating velocity above 1000 rpm would be an essential setting in the measurement such as polarization characteristics [8].

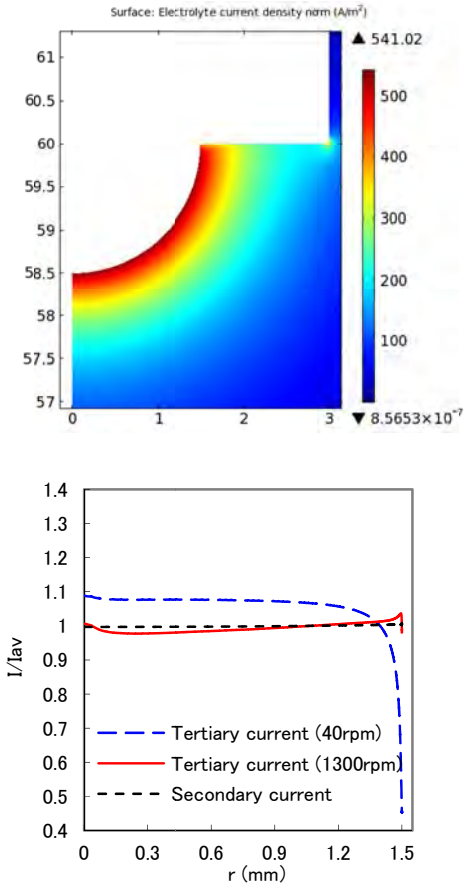

Figure 9. Tertiary current distribution at a hemispherical working electrode in comparison with secondary current distribution. I_{av} is the average current density over the working electrode.

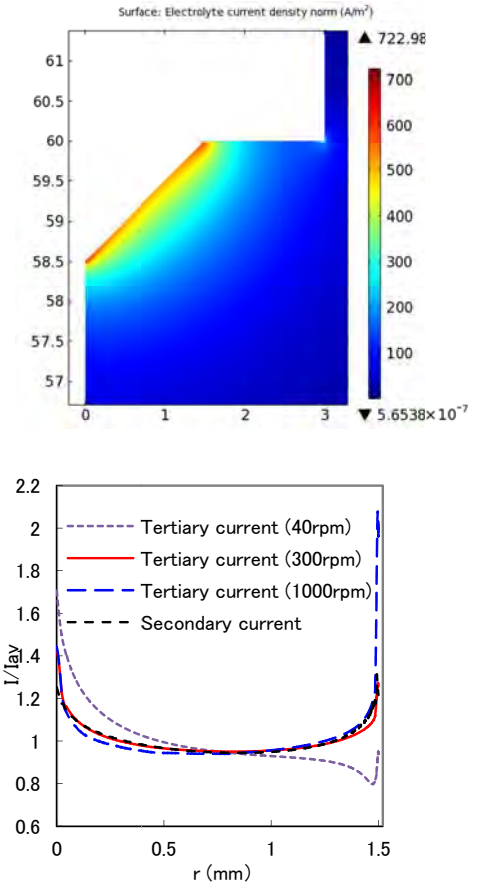

Figure 10. Tertiary current distribution at the inverted cone working electrode in comparison with secondary current distribution. I_{av} is the average current density over the working electrode.

3.3 Tertiary current distributions at the different types of working electrode

In this work, a hemispherical working electrode and an inverted cone working electrode [1] are used to study the effect of shapes of working electrode on current distributions. The tertiary current distributions at a hemispherical working electrode are shown in Fig. 9, which are comparison with secondary current distribution. The property of more uniform current distribution on the working electrode is demonstrated at ω = 1300 rpm, which agrees well with the secondary current distribution. It is found that at a low rotating velocity such as 40 rpm, the effect of fluid flows to the current distribution is large and then the tertiary current distributions at working electrode are quite different from the secondary current distribution.

Figure 10 shows the tertiary current distributions at an inverted working electrode, in which the effect of fluid flows to the current distributions is large. The appropriate rotating velocity is found to be 300 rpm. The further increase of rotating velocity will cause the more non-uniform, which is quite different from the case of hemispherical working electrode.

The usage of hemispherical working electrode allows us to obtain more uniform current distributions over the whole surface of working electrode. Since the diameter of commercial planar working electrode considered is 3 mm, as shown in Fig. 8, the uniform current distributions are located within the domain with

a diameter of 2 mm, *i.e.*, less than 1/2 of surface area of working electrode, which is a strict dimension for measurement such as polarization characteristics [8]. It could thus be proposed that the substitution of hemispherical working electrode for planar working electrode would improve the accuracy of practical measurement.

4. Conclusions

This paper presented the study of tertiary current distributions on rotating electrodes. The coupled solution of fluid equations and mass-transport equations were performed. The concentration distributions were obtained and the calculated concentration boundary layer thicknesses agreed well with those of Levich equation. The comparison of the tertiary current distributions with the secondary current distributions demonstrated that the control of the rotating velocity could reduce the effect of fluid flows.

Simulations demonstrated that a practical range of fluid dynamics, concentration distribution, concentration boundary layer, tertiary current distribution, and secondary current distribution were achievable in the electrochemical cell employing a rotating electrode. The study of the current distributions for different types of working electrode indicated that the hemispherical working electrode would be a better choice to improve the accuracy of measurement.

5. References

1. D.R. Gabe, "Rotating electrodes for use in electrodeposition process control", *Plating & Surface Finishing* **82**, 69-76 (1995)
2. Q. Dong, S. Santhanagopalan, R.E. White, "A comparison of numerical solutions for the fluid motion generated by a rotating disk electrode", *J. Electrochem. Soc.*, **155** (9), B963-B968 (2008)
3. O.E. Barcia, L.S.R. Lamego, O.R. Mattos, B. Tribollet, "The modulated flow at a rotating hemispherical electrode", *J. Electrochem. Soc.*, **148** (1), C1-C9 (2001)
4. L.Z. Tong, K. Ohara, F. Asa, Y. Sugiura, "CFD analysis of eductor agitation in electro-plating tank", *Trans. Inst. Met. Finish.*, **88**(4), 185-190 (2010)
5. J.S. Newman, K.E. Thomas-Alyea, *Electro-chemical systems*, 3rd ed., John Wiley & Sons, Hoboken, NJ (2004)
6. A.F. Averill, H.S. Mahmood, "Determination of tertiary current distribution in electro-deposition cells – Part 1 Computational techniques", *Trans. Inst. Met. Finish.*, **75**(6), 228-233 (1997)
7. C.T.J. Low, E.P.L. Roberts, F.C. Walsh, "Numerical simulation of the current, potential and concentration distributions along the cathode of a rotating cylinder Hull cell", *Electrochim. Acta* **52**, 3831-3840 (2007)
8. L.Z. Tong, K. Ohara, F. Asa, Y. Sugiura, "Effect of flow velocity and metal ion concentration on polarization characteristics in electroplating", *122th* Symposium *of The Surface Finishing Society of Japan*, Sendai, Japan, Sep. 2010. Proceedings: 57 (*in Japanese*)
9. Ph. Mandin, Th. Pauporté, Ph. Fanouillère, D. Lincot, "Modelling and numerical simulation of hydrodynamical processes in a confined rotating electrode configuration", *J. Electroanalyt. Chem.*, **565**, 159-173 (2004)
10. COMSOL Multiphysics 4.2- user's guide for CFD Module and Electrodeposition Module and also http://www.comsol.com
11. S. Toshima, H. Sasaki, *Electrochemistry*, rev. ed., The Institute of Electrical Engineers of Japan, Tokyo, Japan (1987) (*in Japanese*)